Analyst

PAPER

View Article Online
View Journal | View Issue

Cite this: *Analyst*, 2016, **141**, 1421

Amplification-free *in situ KRAS* point mutation detection at 60 copies per mL in urine in a background of 1000-fold wild type†

Ceyhun E. Kirimli,[a] Wei-Heng Shih[b] and Wan Y. Shih*[a]

We have examined the *in situ* detection of a single-nucleotide *KRAS* mutation in urine using a $(Pb(Mg_{1/3}Nb_{2/3})O_3)_{0.65}(PbTiO_3)_{0.35}$ (PMN-PT) piezoelectric plate sensor (PEPS) coated with a 17-nucleotide (nt) locked nucleic acid (LNA) probe DNA complementary to the *KRAS* mutation. To enhance the *in situ* mutant (MT) DNA detection specificity against the wild type (WT), detection was carried out in a flow with a flow rate of 4 mL min^{-1} and at 63 °C with the PEPS vertically situated at the center of the flow in which both the temperature and the flow impingement force discriminated the wild type. Under such conditions, PEPS was shown to specifically detect *KRAS* MT *in situ* with 60 copies per mL analytical sensitivity in a background of clinically-relevant 1000-fold more WT in 30 min without DNA isolation, amplification, or labeling. For validation, this detection was followed with detection in a mixture of blue MT fluorescent reporter microspheres (FRMs) (MT FRMs) that bound to only the captured MT and orange WT FRMs that bound to only the captured WT. Microscopic examinations showed that the captured blue MT FRMs still outnumbered the orange WT FRMs by a factor of 4 to 1 even though WT was 1000-fold of MT in urine. Finally, multiplexed specific mutation detection was demonstrated using a 6-PEPS array each with a probe DNA targeting one of the 6 codon-12 *KRAS* mutations.

Received 5th October 2015,
Accepted 26th December 2015

DOI: 10.1039/c5an02048d

www.rsc.org/analyst

Introduction

Cancer is a genetic disease and gene mutation is an important form of genetic defects that play a central role in cancer pathways. Detecting gene mutation is essential for cancer diagnosis, therapy decision, and therapy efficacy monitoring. The challenge for gene sequencing from solid tumor samples is that therapeutic decision making based on a single biopsy can be very difficult due to tumoural heterogeneity.[1] Furthermore, the biopsy procedures used for removing tissues from cancers of the internal organs are highly intrusive and expensive and not performed in some cases due to the increased risk of tumour seeding at other sites.[2] These shortcomings make it highly desirable if body fluids such as blood or urine can be used for cancer genetic marker detection.

Polymerase chain reaction (PCR) has been the method for detecting circulating deoxyribonucleic acid (DNA) markers in a serum or urine. To detect gene mutation, PCR is typically followed with melting temperature analysis to differentiate a mutant (MT) from the wild type (WT), the normal form of the gene. So far, detecting mutations in sera or urine has been challenging because (1) the melting-temperature difference between a single-nucleotide MT and the WT can be only a few degrees,[3] (2) the concentrations of circulating MT markers are exceedingly low (much lower than 10^{-18} M or 600 copies per mL),[4] (3) circulating MT markers are typically outnumbered by the WT by a factor of 240 or larger,[5] (4) *trans*-renal DNA exist in urine in the form of short fragments often less than 200 base pairs (bp),[6] and PCR suffers from the amplicon size, where only a small amount of the naturally occurring fragments in urine can be amplified.[5,7] These combinations make it difficult to detect circulating mutations sensitively and specifically. Therefore, if there is a genetic detection method that can detect genetic mutations in short DNA fragments of less than 200 bp at concentrations lower than aM (10^{-18} M) and in a background of more than 240-fold wild type (WT) without the need for DNA isolation or amplification it would be ideal for reliably detecting circulating genetic mutations in urine and this can greatly help cancer diagnostics and treatment decision and monitoring.

Genetic detection technologies currently under development rely on fluorescence,[8] quartz crystal microbalance (QCM),[9,10] electrochemical[11] binding to nano-metal particles,[12]

[a]*Drexel University, School of Biomedical Engineering, Science, and Health Systems, Philadelphia, Pennsylvania 19104, USA. E-mail: shihwy@drexel.edu*
[b]*Drexel University, Department of Materials Science and Engineering, Philadelphia, Pennsylvania, USA*

†Electronic supplementary information (ESI) available. See DOI: 10.1039/c5an02048d

surface plasmon resonance (SPR),[13] silicon-based microcantilever sensors as well as piezoelectric microcantilever sensors. For DNA detection, nanoparticle-amplified QCM exhibited a concentration sensitivity of 1 pM.[14] Nanoparticle enhanced SPR exhibited a concentration sensitivity of 10–100 aM.[15] The electrochemical methods involving nanofibers and nanotubes also exhibited a concentration sensitivity of the order of 30 fM.[16] Nanowires,[17–21] and nanotubes[22,23] exhibited a concentration sensitivity ranging from 100 fM to 1 fM. Microcantilevers coupled with nano-metal particles exhibited a 0.01 nM concentration sensitivity.[24] Although many of these methods such as QCM, SPR, silicon-based microcantilever sensors as well as lead zirconate titanate (PZT) piezoelectric microcantilever sensors (PEMS)[25,26] are label-free, the sensitivity was still many orders of magnitude away from the attomolar (aM, or 10^{-18} M) requirement. Similarly, the 10^{-16} M sensitivity achieved by magnetic bead isolation coupled with electrochemical enhancement was still not sufficient.[27] Nano-scale mechanical imaging by atomic force microscopy (AFM) could differentiate unhybridized single-stranded DNAs (ssDNAs) from hybridized double-stranded DNAs (dsDNAs) at aM sensitivity but it required a sophisticated instrument such as AFM.[28] Carbon nanotube impedance biosensors exhibited a 100 aM sensitivity in DNA detection, which was insufficient for clinical applications.[29] GaN nanowire extended-gate field-effect-transistors[30] and streptavidin horseradish peroxidase functionalized carbon nanotubes[31] have aM sensitivity in DNA detection. However, these detections are not *in situ*, they typically require washing steps before the measurements can be made. Peptide nucleic acid (PNA) probe-enhanced electrochemical biosensors that were based on an integrated chip also exhibited aM sensitivity. However, they also required washing.[32] Recently a disposable electrochemical biosensor based on magnetic bead amplification and target DNA biotinylation exhibited aM sensitivity.[33] However, it required multiple steps of amplification and the need to biotinylate the target DNA renders it impractical.[33] In comparison with these technologies, the limit of detection (LOD) of a piezoelectric plate sensor PEPS in urine exceeds the attomolar level requirement while it is also label-free. Moreover detection with PEPS provided enough specificity for mutant target DNA on a background of 250 times more wild type target DNA.[34]

A lead magnesium niobate–lead titanate $(Pb(Mg_{1/3}Nb_{2/3})O_3)_{0.65}(PbTiO_3)_{0.35}$ (PMN-PT) piezoelectric plate sensor (PEPS) consists of a PMN-PT freestanding film 8 μm in thickness[35] thinly coated with gold electrodes on the two major surfaces and encapsulated with a thin electrical insulation. By covalently immobilizing a probe DNA (probe) complementary to a target DNA and immersing the probe-coated PEPS in a biological fluid sample, binding of the target DNA from the biological fluid sample to the probe on the PEPS surface shifts the PEPS length extension mode (LEM) and the width extension mode (WEM) resonance frequency, f. *In situ* detection of the target DNA from the biological fluid sample has been achieved by monitoring the PEPS LEM[36] or the WEM[37] resonance frequency shift, Δf in real time. The detection signal of PEPS is mainly from the response to surface stress which is larger than the response to mass change by more than 1000 times. The reason for the large response to surface stress is that PEPS can switch its crystalline orientation under the influence of surface stress, which no other materials can. Because the elastic moduli of crystalline materials are orientation-dependent, the resultant elastic modulus change causes a resonance frequency shift more than 1000 times higher than could be obtained by mass change alone.[36,38–42] Using a 200-nucleotide (nt) Hepatitis B virus 1762T/1764A double mutation (HBVDM) as a model single-stranded MT, PEPS has exhibited unprecedented PCR-like 100 zM (10^{-19} M) analytical sensitivity in detecting HBVDM in urine *in situ* and in real time without DNA isolation or amplification.[37]

In view of the high sensitivity and specificity demonstrated by a PEPS in detecting HBVDM which contains two point mutations separated by one nucleotide, the goal of this study is to further investigate the specificity of *in situ* single-nucleotide mutation detection in urine against the WT in real time using a PEPS with a locked nucleic acid (LNA) probe in a flow and with temperature control but without DNA isolation or amplification. *KRAS* mutations are point mutations (PMs) at codons 12 and 13 and less frequently at codon 61 that occur in about 50% of colorectal cancers[43] and more than 80% of pancreatic cancers.[44] Among the seven most common *KRAS* mutations, codon-12 GGT to GTT point mutation (PM) (Glycine to Valine) (G12V) is associated with a higher mortality rate.[45] The frequency of this mutation among *KRAS* mutated colorectal cancers is 21.9–24.4%.[46] In this study we will use the *KRAS* G12V PM as the model PM. Specifically, we will use a 50-nt *KRAS* PM as the model MT. Hybrid probes containing both DNA and locked nucleic acid (LNA) nucleotides have been shown to increase the melting-temperature difference between the MT and WT and enhance the specificity of mutation detection.[47–54]

For the GGT-to-GTT *KRAS* mutation, we designed and immobilized a LNA-containing probe on the PEPS surface to carry out *in situ KRAS* PM MT detection against the WT at a temperature below the melting temperature of the MT but above that of the WT and with a flow rate of 4 mL min^{-1}. We showed that the PEPS positively and specifically detected the *KRAS* G12V PM MT at a concentration of 60 copies per mL (100 zM or 10^{-19} M) in a background of 1000-fold WT and further validated the MT detection by following with *in situ* fluorescent reporter microsphere (FRM) detection and by visualizing the fluorescence colors of FRMs. The numbers of the captured MT FRMs outnumbered the captured WT FRMs by a factor of 4 to 1, indicating the specificity of PEPS single-nucleotide PM detection even when the sample contains 1000-fold WT.

Experimental

Probe, MT, WT, rDNAs and FRMs

The 17-nt LNA probe used to detect the *KRAS* G12V PM MT was a synthetic single-stranded DNA (Exiqon) complementary

Table 1 Sequences of the probe, MT, WT, MTrDNA, and WTrDNA and the melting temperatures (T_m) of MT with probe, WT with probe, MTrDNA with MT, and WTrDNA with WT

Type of DNA	Sequence (5′ → 3′)	T_m
Probe (17 nt)	Amine-(PEG)12-TGGAGCTGTTGGCGTAG	—
MT (50 nt)	TCTGAATTAGCTGTATCGTCAAGGCACTCTTGCCTACGCCA**A**CAGCTCCA	70 °C (probe to MT
WT (50 nt)	CTACGCCA**C**CAGCTCCAACTACCACAAGTTTATATTCAGTCATTTTCAGC	55 °C (probe to WT)
MTrDNA (33 nt)	GCAAGAGTGCCTTGACGATACAGCTAATTCAGA-(PEG)7-Amine	78.5 °C (MTrDNA to MT)
WTrDNA (33 nt)	Amine-(PEG)12-GCTGAAAATGACTGAATATAAACTTGTGGTAGT	73.6 °C (WTrDNA to WT)

Note that the site where the mutation occurs is indicated by a bold letter in the MT, WT, and probe and the LNA bases in the probe are underlined. The melting temperatures were estimated using a 115 mM salt concentration consistent with the urinary salt content[56,57] and a LNA/DNA concentration of 50 nM.

to the sequence of the *KRAS* gene (Gene ID: 3845) centered around the *KRAS* G12V PM with the 3 LNA bases also centered around the PM as shown in Table 1. Such a design has been shown to increase the melting-temperature difference between the binding of the MT to the probe and that of the WT to the probe.[55] Without using the 3 LNA bases, the melting temperatures of the MT and the WT would be 62 °C and 52 °C, respectively with a melting temperature difference of 10 °C. With the 3 LNA bases, the melting temperature of the MT was 70 °C and that of the WT 55 °C. The melting-temperature difference between the MT and the WT was thus increased from 10 °C to 15 °C. The probe was amine-activated with a 12-polyethyleneglycol (PEG) spacer at the 5′ end. The sequence of the probe is shown in Table 1. The MT and WT were 50-nt long synthetic single-stranded DNA (Sigma). The MT contained a sequence complementary to the probe at the 3′ end plus 33 nt of the immediately upstream sequence while the WT contained the sequence complementary to the probe at the 5′ end except for the point mismatch plus 33 nt of the immediately downstream sequence. Also shown in Table 1 is the sequence of the rDNA for MT (MTrDNA) which was complementary to the upstream sequence of the MT in Table 1 and the sequence of the rDNA for WT (WTrDNA) complementary to the downstream sequence of the WT in Table 1. Both MTrDNA and WTrDNA were 33-nt long (Sigma). The WTrDNA was amine activated with a 12-PEG spacer at the 5′ end and the MTrDNA was also amine activated but with a 7-PEG spacer at the 3′ end. Also shown in Table 1 are the melting temperatures (T_m) for the binding of the MT with the probe, that for the binding of the WT with the probe, that for the MTrDNA to MT, and that for the WTrDNA to WT. MTrDNA and WTrDNA were covalently conjugated to the MT FRMs and WT FRMs, respectively. Both MT and WT FRMs were 6 μm in size but differed in the fluorescence color. MT FRMs emitted blue light (Bright Blue (BB) (≅ Coumarin), Polysciences) with the excitation maximum at 360 nm and the emission maximum at 407 nm whereas the WT FRMS emitted yellow-green light (Yellow Green (YG) (≅ Fluorescein), Polysciences) with the excitation maximum at 441 nm and the emission maximum at 486 nm. Fig. 1 shows a schematic illustrating the relationship between the probe, MT, WT, MTrDNA, WTrDNA, MT FRMs, and WT FRMs. As can be seen, the sequences of MT, WT, MTrDNA, and WTrDNA were chosen such that the MT FRMs would report only the presence of MT and the WT FRMs would report only the presence of WT. For this purpose, after FRM detection, two fluorescence images of the PEPS surface were taken using an Olympus BX51 fluorescence microscope using the imaging procedure described earlier.[58] One image contained only the MT FRMs by using a D350/50 filter (Chroma) for excitation and a 400 nm long-pass filter (Chroma) for emission while the other image contained only the WT FRMs by using a D460/50 filter (Chroma) for excitation and a HQ545/30 filter (Chroma) for emission. Even though the MT FRM images were taken with a 400 long pass emission filter, they did not contain the images of WT FRMs because the WT FRMs could not be excited with the D350/50 excitation filter. For the latter image, a longer exposure time was used to make up for the fact that the emission filter did not completely overlap with the emission spectrum of the WT FRMs. The fluorescence spots in the MT FRM image were then colored blue to denote that they are MT FRMs and those in the WT FRM image were then colored orange to denote that they are WT FRMs using MatLab. After coloring, the blue and orange images were merged using MatLab. Because MT FRMS and WT FRMS exhibited different fluorescence colors, by examining the colors of the FRMs captured on the PEPS surface following MT detection in a mixture of MT and WT, one could determine how specific the MT detection was in a background of WT.

PEPS fabrication and electrical insulation

The PEPS used in this study was 1.2 mm long and 0.45 mm wide, fabricated from $(PbMg_{1/3}Nb_{2/3}O_3)_{0.65}(PbTiO_3)_{0.35}$ (PMN-PT) freestanding films 8 μm in thickness, that was coated with a 110 nm thick Cr/Au electrode by thermal deposition (Thermionics VE 90) cut into 2.5 mm by 0.45 mm strips by a wire saw (Princeton Scientific Precision, Princeton, NJ) as shown in Fig. 2a. Gold wires, 10 μm in diameter, were glued to the top and bottom electrodes of each strip using a conductive glue (XCE 3104XL, Emerson and Cuming Company, Billerica, MA). The rear end of the strip was fixed on a glass substrate by a nonconductive glue (Loctite 1C Hysol Epoxy Adhesive) to form the PEPS geometry and poled at 15 kV cm^{-1} at 90 °C for

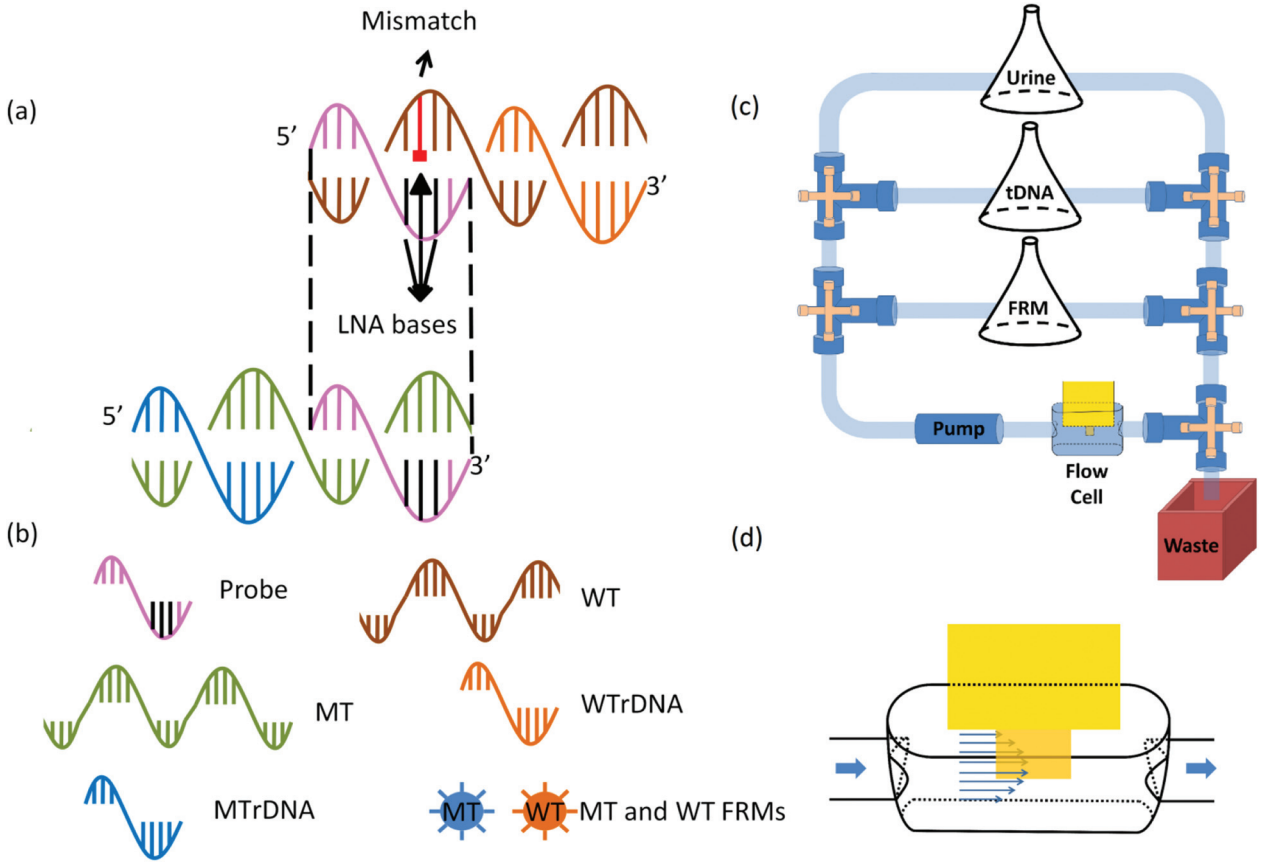

Fig. 1 (a) A schematic of the relationship between the probe, mutant (MT) target DNA, wild type (WT), MT reporter DNA (MTrDNA), and WT rDNA (WTrDNA) for *KRAS* point mutation, (b) the legend for the schematic in (a), (c) a schematic of the flow system for mutation detection in urine and (d) a blow-up of the PEPS situated in the center of the flow cell.

60 min in an incubator (Digital Control Steel Door Incubator 10–180E, Quincy Lab). The dielectric constant of the PEPS was measured using an electrical impedance analyzer (Agilent 4294A) to be about 1800 with a loss factor of 2.8% at 1 kHz. The PEPS was electrically insulated to stabilize the resonance peaks for in-liquid detection by using a new 3-mercaptopropyl-trimethoxysilane (MPS) (Sigma-Aldrich Co. LLC.) solutions coating scheme involving enhanced MPS cross-linking at pH = 9.0 and with the addition of water as described before.[59] The MPS insulation also served as the anchor to immobilize the probe *via* the bi-functional linker SMCC. The pK_a of thiols is about 10.5. Under coating conditions at pH = 9.0 or immobilization conditions at pH = 7, most of the thiols were un-oxidized and good for immobilization. Indeed, the probe immobilized on the MPS surface was quantified using a quartz crystal microbalance (QCM) to be about 3–4 probes per 100 nm^2.[60] Thus, the SH of the MPS was proven to be effective to facilitate the immobilization of the probe DNA. A schematic of LEM vibrations and that of WEM vibrations of a PEPS is shown in insets (I) and (II) of Fig. 2b, respectively. The impedance (blue) and phase angle (red) *versus* frequency resonance spectra around the first WEM peak frequency—which was taken as the peak frequency of the phase angle *versus* the frequency spectrum—are shown in Fig. 2b. Because the phase-angle resonance spectrum was much more symmetric than that of the impedance, in the following, all detections were carried out using the phase-angle spectrum to track the WEM peak.

Probe immobilization, nonspecific binding blocking, and FRM conjugation

Sulfosuccinimidyl-4-(*N*-maleimidomethyl)cyclohexane-1-carboxylate (sulfo-SMCC) (Pierce) was first dissolved in water followed by dilution in a phosphate buffer saline (PBS) solution. To immobilize the amine-activated probe on the PEPS surface, the MPS-coated PEPS was first immersed in 200 μL of a 5 mM sulfo-SMCC solution in PBS with the pH adjusted to 6.5 for 1 hour. The sensor was then washed three times with deionized water and then it was immersed in a solution of 10 μM of amine activated probe dissolved in 200 μL of PBS (pH 8.0). A schematic illustrating the immobilization of the amine-activated probe on the PEPS surface *via* the thiol functionality of the MPS insulation layer is shown in Fig. S1 of the ESI.† After probe immobilization, the PEPS was treated with 3% bovine serum albumin (Sigma) in PBS for 1 h followed by washing 5 times with PBS. As demonstrated by the previous study, 3% BSA was sufficient to completely block the nonspecific

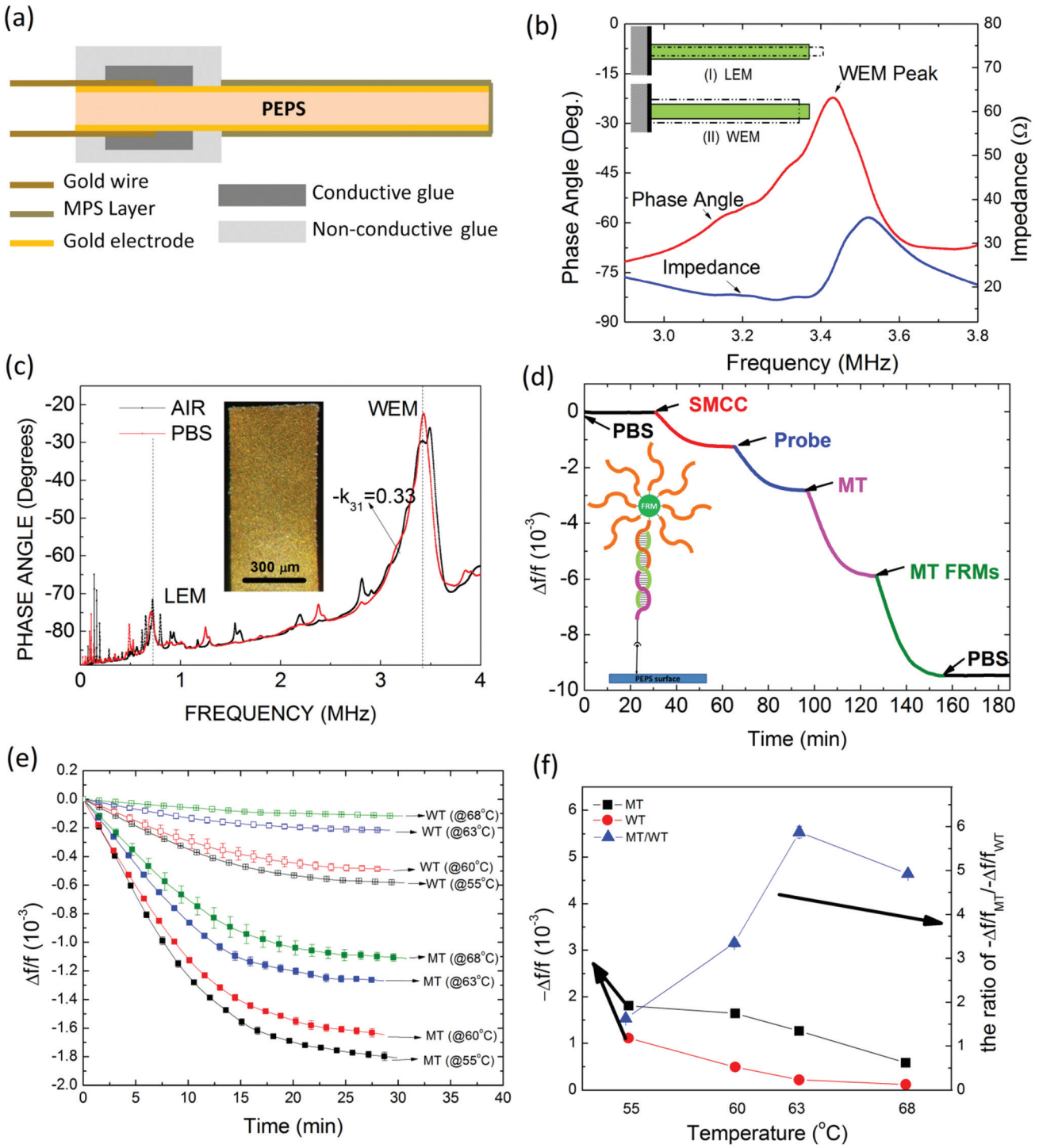

Fig. 2 (a) A schematic of the side view of the PEPS. The gold wires were connected to the top and bottom gold electrodes with conductive glue. The entire rear end including the conductive glue was covered with non-conductive glues. MPS layer covered the front end of the PEPS that was not covered by the nonconductive glue. (b) The blowup of both the impedance-*versus*-frequency (blue) and phase angle-*versus*-frequency (red) spectra around the WEM resonance peak around 3.4 MHz. Also included are schematics for LEM and WEM vibrations in insets (I) and (II), respectively. (c) In-air (black) and in-PBS (red) phase angle-*versus*-frequency resonance spectra with an inset showing an optical micrograph of the PEPS, and (d) relative resonance frequency shift, $\Delta f/f$, of the PMN-PT PEPS going through the PBS step (0–30 min), the SMCC bonding step (30–60 min), the probe immobilization step (60–90 min), the MT detection step (90–120 min), the MT FRM detection step (120–150 min), and the final PBS step (150–180 min) with an inset showing a schematic of the molecules involved in these steps. (e) MT (solid symbols) and WT (open symbols) detection at 1×10^{-15} M in PBS at 55 °C (black), 60 °C (red), 63 °C (blue) and 68 °C (green) for 30 min, (f) average $-\Delta f/f$ at 25–30 min *versus* temperature, squares for MT and circles for WT. Also plotted is the ratio of the average $-\Delta f/f$ at 25–30 min of the MT to that of the WT (triangles) (the right side of the double-y plot).

bindings for DNA detection in urine.[37] The MT FRMs were covalently conjugated to MTrDNA and the WT FRMS to the WTrDNA using procedures described previously.[36,58] The total volume of the MT FRM solution was 8 mL and the concentration was 1×10^5 FRMs per mL. At 2 mL min^{-1}, this solution was recycled approximately 7 times in the 30 minutes of the MT FRM detection step. The likely reason for the fact that the detection of the 50-nt MT/WT produced a quite similar $\Delta f/f$ to that of the detection of the larger MT FRMs/WT FRMs is the following. DNA was highly negatively charged—including the probe DNA on the PEPS surface, MT, WT and the reporter DNA on the FRM surface. Therefore, much of the surface stress generated by MT, WT or FRM binding was due to the electrostatic repulsive forces between the negatively charged surface due to the immobilized probe DNA layer and the negatively charged target (MT, WT or FRMs). Under physiological electrolyte concentrations, the electrical screening length (or electrical double layer thickness) is less than 1 nm. This means that charges at a distance more than 1 nm away from the probe DNA layer would generate negligible repulsive forces on the probe DNA layer, and hence on the PEPS surface. As a result, most of the bound FRM did not contribute to the surface stress except for the vicinity at and around the binding site that was right on the probe DNA layer. Note that a 6-μm FRM generated a comparable resonance frequency shift to that of a 50 nt MT or WT which is another indication that the PEPS sensing mechanism is not by mass change.

Spiked urine samples and flow setup

The flow system for carrying out the detection contained a peristaltic pump (Cole-Parmer 77120-62), a flow cell where detection took place, reservoirs containing DNA-spiked urine samples, FRMs, and PBS interconnected with tubing of a 0.8 mm inner diameter as schematically shown in Fig. 1c. The flow cell was 18.5 mm long, 3.5 mm wide and 5.5 mm deep (volume = 356 μL) connected to the sample reservoir. A schematic of the flow cell is shown in Fig. 1d. The total internal volume of the flow cell plus tubing was approximately 750 μL. The urine came from one individual. The subject was free of HBV infection. The urine samples were collected in a "First Morning Specimen" manner, *i.e.*, the bladder was emptied before bed and the sample was collected first thing in the morning. A total of 11 such urine samples were collected for the study and visually there was no significant difference among these 11 urine samples and 21 more that were used for previous studies.[34,37] The flow was driven by the peristaltic pump and what flowed through the flow cell was controlled by the valves. In each detection experiment, the volume of the DNA-spiked urine sample was fixed at 50 mL and the probe-coated PEPS was placed in the center of the flow cell. The flow setup was placed inside an incubator (Digital Control Steel Door Incubator 10–180E, Quincy Lab) for temperature control. Because the flow cell was open a 2-litre water bath was included in the incubator to eliminate a potential resonance frequency shift due to the changes in the flow-cell liquid level by evaporation. The resonance spectra were measured using a portable AIM 4170C impedance analyzer (Array Solutions).

Results and discussion

Single-PEPS mutation detection

An optical micrograph of the PEPS used for this study is shown as an inset in Fig. 2c. The in-air and in-PBS phase angle *versus* frequency resonance spectra of the PEPS are shown in Fig. 2c. As can be seen, the base-line, the length-extension-mode (LEM) resonance peak, and the width-extension-mode resonance (WEM) peak of the in-liquid spectrum were close to those of the in-air spectrum, indicating the effectiveness of the MPS insulation coating. In all of the following experiments, the WEM peak of the phase-angle spectrum was monitored for detection. The relative resonance frequency shift, $\Delta f/f$, of the first WEM peak during the SMCC bonding (30–60 min), the probe immobilization (60–90 min), the subsequent MT detection at 100 pM in PBS (90–120 min) and the following MT FRM detection at a 1×10^5 FRMs per mL concentration in PBS (120–150 min), both at 2 mL min^{-1} are shown in Fig. 2d. Also shown in the inset in Fig. 2d is a schematic of the various steps involved in the immobilization process. Fig. 2d illustrates that the various binding steps that were carried out in PBS at room temperature during surface functionalization, MT detection or FRM validation could be detected by the resonance frequency shift of the PEPS. For actual MT or WT detection in urine, there was a bovine serum albumin (BSA) blocking step right after probe immobilization in which the probe-coated PEPS was treated with a 3% BSA solution for 30 min to saturate any possible nonspecific binding sites such that no nonspecific binding could occur during detection in urine as described earlier.[37]

With the melting temperature for the binding of the MT to the probe being 70 °C and that for the WT to the probe being 55 °C, we carried out the detection of 1×10^{-15} M of MT and WT in PBS at 55 °C, 60 °C, 63 °C and 68 °C for 30 min to find the optimal temperature for specific MT detection against the WT. Three experiments were carried for each condition. The resultant relative detection resonance frequency shift, $\Delta f/f$ is plotted with standard deviations in Fig. 2e. We then averaged out the $\Delta f/f$ of each detection over 25–30 min. The resultant $-\Delta f/f$ at 25–30 min is plotted in Fig. 2f with squares representing MT and circles representing WT (the left side of the double-y plot). The ratio of the $-\Delta f/f$ at 25–30 min of the MT to that of the WT is also plotted in Fig. 2f as triangles (the right side of the double-y plot). As can be seen the ratio of the $-\Delta f/f$ at 25–30 min of the MT to that of the WT was maximal at 63 °C. Fig. 3a and b show the schematic of the MT detection in urine and that of the following MT FRM detection, respectively. Fig. 3c shows the detection $\Delta f/f$ *versus* time of the MT detection in urine at various MT concentrations followed by the MT FRM detection in PBS at 1×10^5 FRMs per mL. Note that the background signal in blank urine (control) before and after the MT and FRM detection steps was stable as shown in

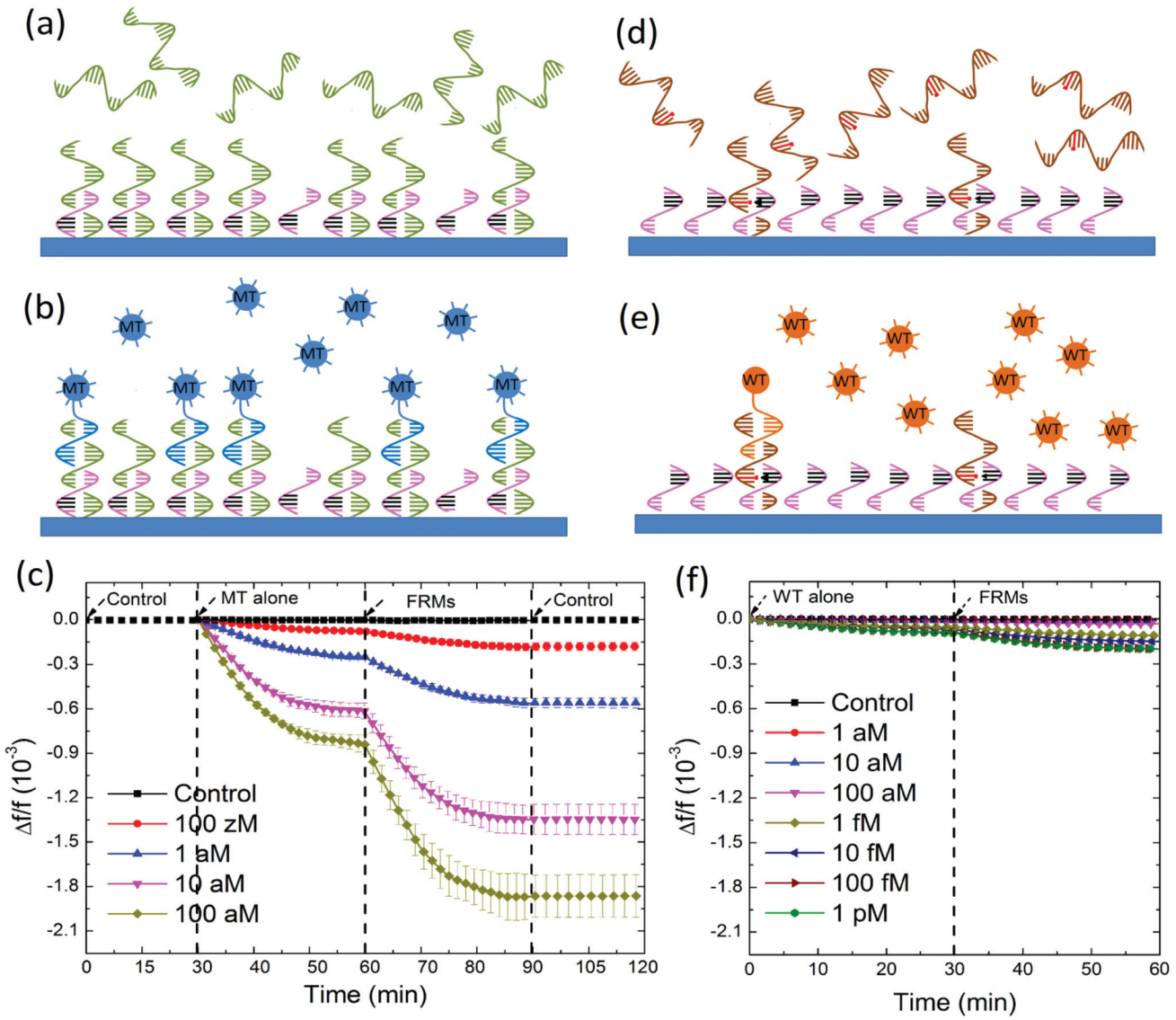

Fig. 3 A schematic representation of (a) MT detection, (b) MT FRM detection following MT detection, (c) $\Delta f/f$ *versus* time of MT detection followed by MT FRM detection including the background signal collection in urine before (0–30 min) and after (90–120 min) the MT and FRM detection, (d) WT detection, (e) WT FRM detection following WT detection, (f) $\Delta f/f$ *versus* time of WT detection followed by WT FRM detection. Clearly, at 63 °C and at a flow rate of 4 mL min^{-1}, the detection $-\Delta f/f$ of 1 aM MT at t = 30 min ($-\Delta f/f = 0.2 \times 10^{-3}$) was much larger than that of WT at 100 fM at t = 30 min ($-\Delta f/f < 0.1 \times 10^{-3}$), indicating the specificity of the MT detection under such detection conditions.

Fig. 3c in all the detection experiments. For simplicity, in all the following figures we will omit the background signal sections to better highlight the detection results. Fig. 3d and e show the schematic of the WT detection in urine and that of the following detection of the WT FRMs in PBS, respectively. Fig. 3f shows the detection $-\Delta f/f$ *versus* time in urine at various MT concentrations followed by the detection of the WT FRMs in PBS at 1×10^5 FRMs per mL. Clearly, the detection $-\Delta f/f$ for MT at 1 aM (1×10^{-18} M) at t = 30 min was about 0.2×10^{-3}, which was still larger than the detection $-\Delta f/f$ of $<0.1 \times 10^{-3}$ for WT at 100 fM (1×10^{-14} M) at t = 30 min, indicating the specificity of the MT detection by PEPS under the chosen detection conditions of 63 °C and a 4 mL min^{-1} flow rate.

To see if PEPS detection of *KRAS* MT under the current detection conditions, *i.e.*, 63 °C and a flow rate of 4 mL min^{-1} was indeed sensitive and specific, we carried out MT detection in a background of 1000-fold higher WT at various MT concentrations. In Fig. 4a, we show the $\Delta f/f$ *versus* time of PEPS detection in urine containing a mixture of MT in a background of 1000-fold more WT at various MT concentrations followed by detection in an equal mixture of 10^5 FRMs per mL of MT FRMs and 10^5 FRMs per mL of WT FRMs in PBS.

After detection in the mixture of MT FRMs and WT FRMs and washing, the PEPS was examined using a fluorescence microscope and the obtained fluorescence images from detection at various MT concentrations are shown in Fig. 4b–e

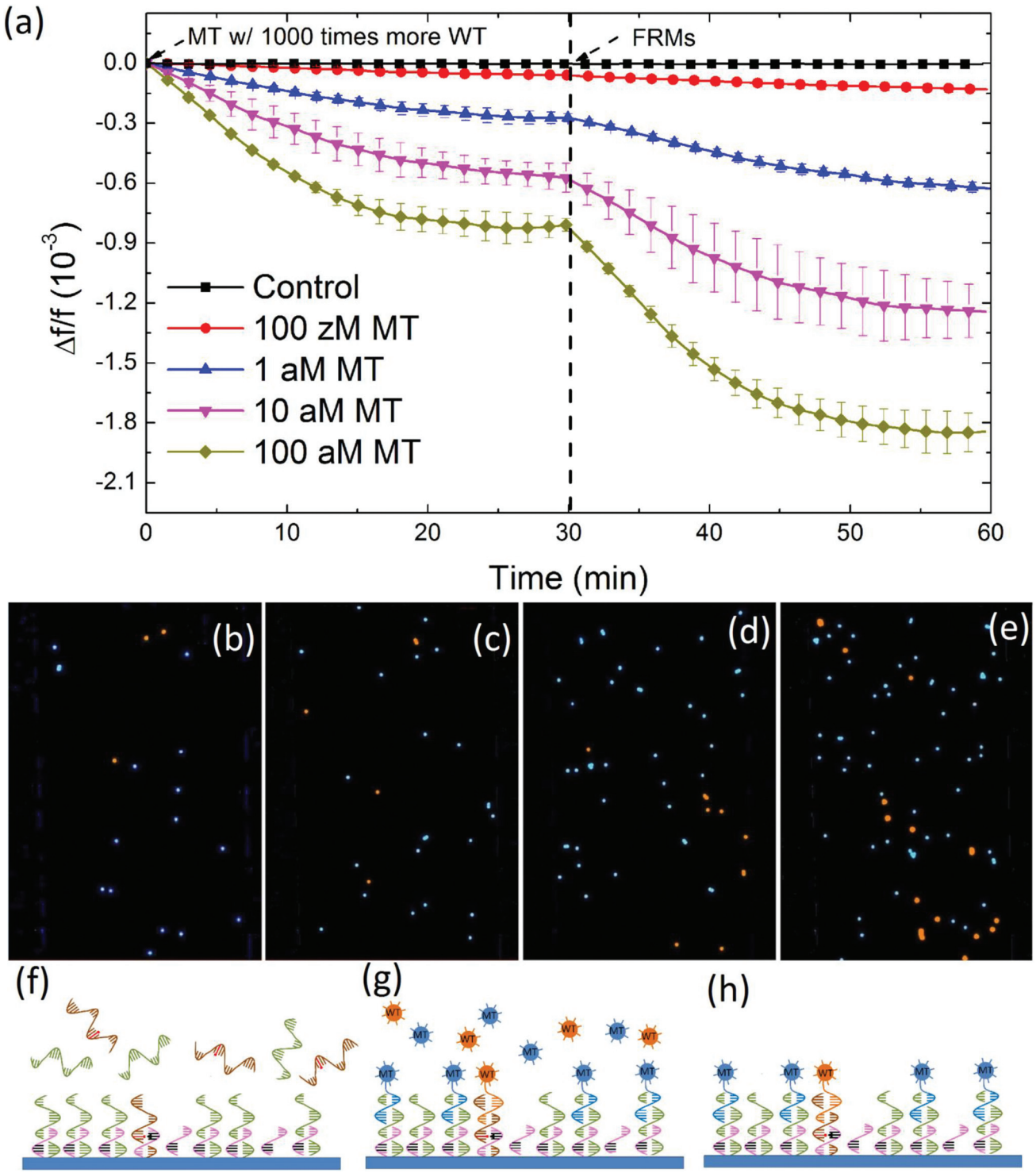

Fig. 4 (a) Relative resonance frequency shift, $\Delta f/f$ *versus* time of the PEPS detection of MT in a background of 1000-fold more WT at various MT concentrations followed by detection in an equal mixture of 10^5 FRMs per mL of MT FRMs and 10^5 FRMs per mL of WT FRMs in PBS, (b), (c), (d), and (e) are respectively the fluorescence images of the PEPS obtained after the FRMS detection following the MT detections at 0.1 aM (100 zM), 1 aM, 10 aM, and 100 aM MT concentrations where the blue color denotes the MT FRMs while the orange color denotes the WT FRMs, (f), (g), and (h) are respectively the schematic illustrating the PEPS in a mixture of MT and WT at t = 0–30 min in (a), a schematic of the PEPS in a mixture MT FRMs and WT FRM at t = 30–60 min in (a), and a schematic of the PEPS after the final washing. That there were far more MT FRMs captured than WT FRMs in (b)–(e) indicates that the detection of MT was specific even in a background of 1000 times more WT.

where the blue spots represent the MT FRMs and the orange ones WT FRMs. As can be seen, in all four MT concentrations (*i.e.*, 100 zM, 1 aM, 10 aM and 100 aM) the blue MT FRMs outnumbered the orange WT FRMs. In addition, both the number of MT FRMs and that of the WT FRMs increased with an increasing MT concentration since the WT concentration was increased in proportion as well. In Fig. 5a, we plot the number of MT FRMs and that of WT FRMs *versus* the average $-\Delta f/f$ of MT detection in a MT/WT mixture as obtained from the $-\Delta f/f$ at t = 25–30 min in Fig. 4a. Clearly, both the number of the MT FRMs and that of the WT FRMs increased roughly linearly with an increasing average $-\Delta f/f$ of MT detection with a MT FRM/WT FRM number ratio of about 4 validated that the $\Delta f/f$ obtained in a MT/WT mixture with a WT/MT ratio of 1000 was mostly due to the binding of MT on the PEPS surface such that the bound FRMs were mostly MT FRMs. These results are schematically illustrated in Fig. 4f–h. Fig. 4f illustrates that even in a mixture of MT with 1000-fold more WT, still more MT than WT were captured on the PEPS surface because the temperature and flow conditions favored MT to bind to the probe on the PEPS surface. Fig. 4g illustrates that on detection in an equal mixture of MT FRMs and WT FRMs following the detection in the mixture of MT with 1000-fold more WT, more MT FRMS would bond on the PEPS surface due to more MT captured on the PEPS surface. Fig. 4h illustrates that the final PEPS surface had more bound MT FRMs with a MT FRM/ WT FRM number ratio of about 4 after detection in the equal mixture of MT FRMs and WT FRMs and washing.

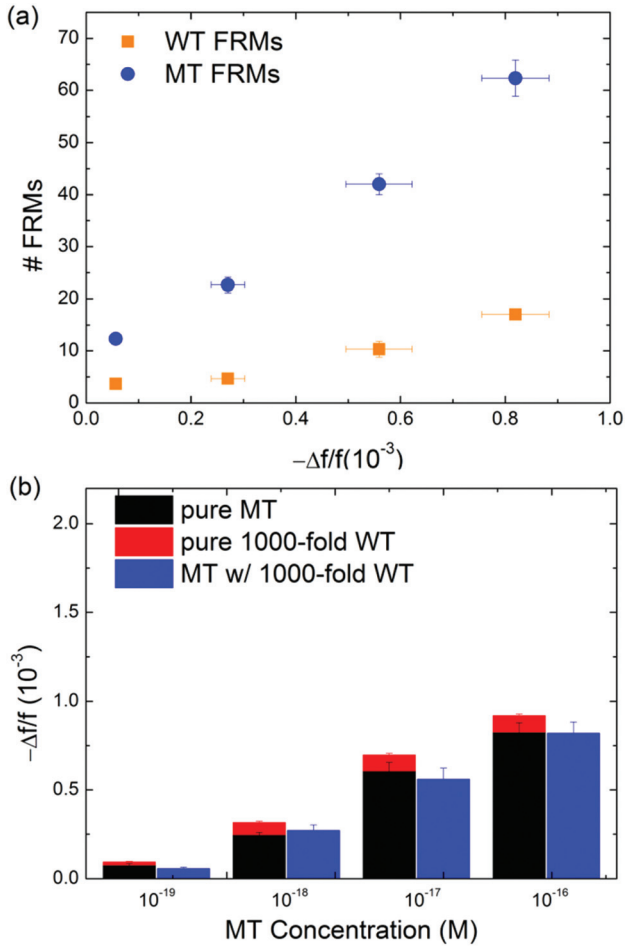

Fig. 5 (a) Number of MT FRMs (blue full circles) and that of WT FRMs (orange full squares) obtained from (b)–(e) *versus* average PEPS MT detection $-\Delta f/f$ at t = 25–30 min taken from Fig. 4(a). Note that for each MT concentration the number of MT FRMs (blue) was still roughly 4 times higher than that of the WT, even the concentration of the WT was 1000 times higher than that of the MT. This indicates that in each case more than 80% of the detection $\Delta f/f$ was due to the binding of the MT and that PEPS's MT detection was specific even if the concentration of the WT was 1000 times higher than that of the MT. (b) Comparison of $-\Delta f/f$ for detection averaged over t = 25–30 min of pure MT in Fig. 4(c) (black), that at 1000-fold pure WT taken from Fig. 4(f) (red) and that in a mixture of MT in 1000-fold more WT as taken from (a) (blue). That the $-\Delta f/f$ in a mixture of MT in 1000-fold WT (blue) was similar to the sum of the $-\Delta f/f$ of MT and the $-\Delta f/f$ of 1000-fold more WT indicates that the presence of the 1000-fold WT had a negligible effect on the MT detection. In addition, the $-\Delta f/f$ of pure MT (black) was also roughly 4 times that of 100-fold pure WT (red), further confirmed the specificity of the current PEPS single-nucleotide mutation detection.

To see how the detection of MT in a background of 1000-fold WT shown in Fig. 4a compared with detection in pure MT and that in pure WT in Fig. 3c and f , we plot in Fig. 5b the average $-\Delta f/f$ over t = 25–30 min at 10^{-19} M, 10^{-18} M, and 10^{-17} M in pure MT (black) as obtained from Fig. 3c, that at 1000-fold WT (red) as obtained from Fig. 3f, and that in a mixture of MT with 1000-fold WT (blue) as obtained from Fig. 4a (blue). As can be seen from Fig. 5b, the overall detection $-\Delta f/f$ in a mixture (blue) was somewhat smaller than that of pure MT detection at the same concentration (black), understandably due to the interference by the presence of the 1000-fold WT except at low concentrations where WT had a negligible effect due to the low concentrations.

Note in Fig. 5b, the $-\Delta f/f$ of the pure MT detection (black) of all three concentrations was also roughly 4 times that of the pure WT detection at a 1000-fold higher concentration, consistent with the results of the detection in the MT/WT mixture as shown in Fig. 5a further supporting that under detection conditions of 63 °C and 4 mL min^{-1}, roughly 80% (4 out of 5) of the detection signals were due to MT even in a background of 1000-fold WT.

Example of 6-PEPS array mutation detection

Codon 12 and codon 13 are hot spots of *KRAS* mutations. Six codon-12 mutations and one codon-12 (G13D) account for more than 98% of all *KRAS* mutations. For the initial demonstration of the PEPS capability of multiplexed mutation detection, we constructed an array of six PEPSs to target the 6 codon-12 hot-spot *KRAS* mutations. The resonance spectra of the 6 PEPSs are shown in Fig. S2 in the ESI.† In Table 2, we list the six codon-12 *KRAS* mutations, the corresponding LNA probe sequences (Exiqon), the melting temperature between the probe and its target MT and that between the probe and the WT. The 6 synthetic codon-12 MTs were single-stranded and 90-nt long (Integrated DNA Technologies). The melting temperatures of the MTs ranged from 68 °C to 72 °C and those

Table 2 Codon-12 *KRAS* mutations, corresponding LNA probe sequences, melting temperature of the LNA probe with its corresponding MT and that with the WT, the melting temperature difference between the MT and the WT with the probe, and the PEPSs in the 6-PEPS array that target them

Mutation	Probe	T_m of MT to probe (°C)	T_m of WT to probe (°C)	ΔT_m (°C)	
GGT → AGT (G12S)	Biotin-(PEG)12-TGGAGC**TAG**TGGCGTAG	68	52.7	15.3	PEPS1
GGT → CGT (G12R)	Biotin-(PEG)12-TGGAGC**TCG**TGGCGTAG	71	50.1	20.9	PEPS2
GGT → GAT (G12D)	Biotin-(PEG)12-TGGAGCT**GAT**GGCGTAG	70	54.7	15.3	PEPS3
GGT → GCT (G12A)	Biotin-(PEG)12-TGGAGCT**GCT**GGCGTAG	72	51.1	20.9	PEPS4
GGT → GTT (G12 V)	Biotin-(PEG)12-TGGAGCT**GTT**GGCGTAG	70	54.3	15.7	PEPS5
GGT → TGT (G12C)	Biotin-(PEG)12-TGGAGC**TTG**TGGCGTAG	69	53.3	15.7	PEPS6

[a] Bold letters indicate mutation sites; underlines indicate LNAs. The melting temperatures were estimated using a 115 mM salt concentration consistent with the urinary salt content[56,57] and a LNA/DNA concentration of 50 nM.

of the WTs ranged from 50.1 °C to 54.3 °C with melting temperature differences ranging from 15.3 °C to 20.9 °C. Each PEPS was coated with a different LNA probe as specified in Table 2. The immobilization of each biotin-activated probe to each corresponding PEPS was carried out using the procedures described previously.[37] The detection of each MT using the 6-PEPS array was carried out at 63 °C, a temperature midway between the melting temperatures of all the MT and those of the WT and with a flow rate of 4 mL min^{-1}. Multichannel measurement was accomplished by multiplexing 6 sensors using 1 impedance analyzer and two relay modules (Super4 USB Relay Module, TCTEC Pty Ltd, Australia). The 6 PEPSs are cycled through the impedance analyzer *via* the 2 relay modules. The setup was calibrated to exclude the contribution from the relay modules to the complex impedance of the sensor. A MatLab routine was written to control the relay modules to switch between different PEPSs automatically. Solutions for 6 different target DNAs were prepared separately and flowed through the two flow cells in series each containing 3 PEPSs where each PEPS had a different probe immobilized on its surface as illustrated by the different colors on the PEPS surface as shown in Fig. 6a. Although the multiplexed detection was carried out in urine samples spiked with only one type of MT, it is carried out with the ability to read out all six probes at the same time. In each detection event, only one probe has positive response while all five other probes have negative responses, indicative of the accuracy and specificity of the probes. The detection data of each PEPS were collected, analyzed and displayed in real time using the MatLab program in the same way as with a single PEPS. In each detection event, the urine was spiked with only one MT at 100 aM (10^{-16} M). Thus, only the PEPS coated with the complementary probe could detect the MT. Indeed, in Fig. 6b, we show the $\Delta f/f$ *versus* time of the multiplexed detection where there were six $\Delta f/f$ *versus* time plots stacked vertically from (i) to (vi), each plot representing the $\Delta f/f$ *versus* time of one PEPS (PEPS1 to PEPS6). The six detection events were run successively with each event lasting for 30 min. The 6 detection events were denoted by 6 different colors in the plots. As can be seen, each PEPS detected only one mutation but not the others. This example clearly illustrates that array PEPS could perform a

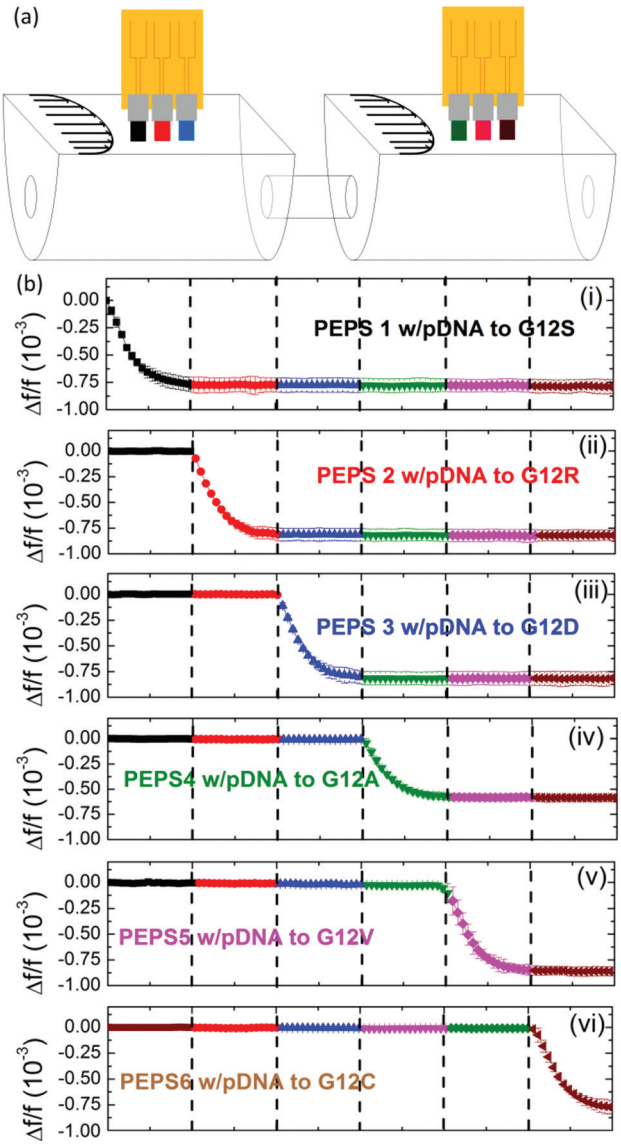

Fig. 6 (a) A schematic of a 6-PEPS array in two flow cells to detect 6 codon-12 *KRAS* mutations and (b) relative frequency shift, f/f *versus* time of an array of 6 PEPSs each coated with a LNA pDNA complementary to one of the 6 codon-12 *KRAS* mutations where 6 different urine samples each spiked with a different 12 *KRAS* mutation (coded with 6 different colors) were flown over the array PEPSs each for 30 min in succession.

multiplexed test to allow all possible forms of the codon-12 mutations to be detected in one single test.

Discussions

There are two types of point mutations, transitions that have no pyrimidine/purine substitutions and transversions with pyrimidine/purine substitutions. Four of the six codon-12 KRAS mutations (G12S, G12D, G12V, and G12C) were transitions and the other two were transversions (G12R and G12A) with a purine substitution of pyrimidine. Using similar probe design considerations such as the number of LNAs, the two transversions had a wider melting temperature spread between MT and WT than the four transitions (see Table 2). In this case, using one of the four transitions, G12V as the model was sufficient to ensure that the same mutation detection methodology could be applied to the two transversions with similar mutation detection specificity as illustrated in the multiplexed detection of all 6 codon-12 KRAS mutations in Fig. 6. For transversions with a pyrimidine substitution of purine which the current study did not consider, using a LNA probe design similar to what was used in the current study could result in a smaller T_m spread between MT and WT. In that case, to widen the T_m spread of such transversions, the LNA probe could be redesigned with a different number of LNAs as well as different locations of the LNAs to allow a T_m spread of 15 °C. With that, the same mutation detection methodology could be applied to such transversions with similar mutation detection specificity as illustrated in this study.

The current probe was only 17-nt long with the mutated site in the middle (9^{th}-nt); as long as the mutation site of a target MT is 8-nt or more from the edge of the target DNA, the binding of the probe to the target MT will have the expected melting temperature of 70 °C. In urine most of the tumor derived cell free DNA fragments have low molecular weight (200 bp).[6] The probability for the mutated site to be within 8 nt of either end would therefore be less than 8% on average. Thus, the current 17-nt probe would bind to the DNA fragments in urine with a probability better than 92%. In comparison, PCR needs two primers and one probe, and thus would not be able to detect a MT with a mutation site as far off the center as 8 nt away from the edge. Conservatively assuming the two primers and the probe to be all 17-nt long, for the MT to be detectable, the mutation site must be 25-nt or more away from the edge, reducing the chances of detecting the MT to 75%. Most of the primer and probe sequences in PCR are much longer than 17-nt, which will further reduce the chance of detecting the mutation from the fragments. Clearly, the current method needs only a short probe is an advantage over PCR in detecting mutations from circulating DNA fragments.

The same methodology should also be able to detect mutations in circulating DNA from plasma or serum. The only difference is that the sensor must be blocked with a higher concentration of bovine serum albumin (BSA) after probe immobilization and prior to detection to prevent non-specific binding as plasma and sera contain higher concentrations of serum albumin.[60]

Finally, the current hybridization temperature is not high enough to denature dsDNA. Detection of dsDNA will require denaturing the dsDNA first prior to hybridization. Both the denaturing step and the hybridization step could be incorporated in the flow system in a continuous fashion and will be published in a future publication.

Conclusion

We have examined the analytical sensitivity and selectivity of the *in situ* detection of gene mutation in urine using a PMN-PT PEPS using *KRAS* G12V point mutation (PM) as the model PM. The PEPS was coated with a 17-nt probe with three LNA bases around the mutated site that was complementary to the *KRAS* PM and the detection was carried out in a flow with the PEPS located at the center of the flow with a flow rate of 4 mL min^{-1} and at 63 °C which was below the melting temperature of the MT with the probe but above that of the WT with the probe. To examine the specificity of the mutation detection in a background of the wild type, we followed the detection in the mixture of MT and WT with the detection in a mixture of MT FRMs and WT FRMs in which MT FRMs and WT FRMs were designed to bind only to MT and WT, respectively. The specificity was further confirmed by visual inspection of the colors of the bound FRMs as the MT and WT FRMs emitted different fluorescence colors. The results indicated that under the optimal detection conditions of 63 °C and 4 mL min^{-1}, PEPS detected the *KRAS* PM with an analytical sensitivity of 60 copies per mL in urine in a background of 1000-fold more WT without DNA isolation or amplification. Counting the captured MT FRMs and WT FRMs after the following FRM detection indicated that roughly 80% (4/5) of the detection signals were due to the MT even in the presence of 1000-fold more WT. Multiplexed mutation detection was demonstrated using a 6-PEPS array each with a probe complementary to one of the 6 codon-12 *KRAS* mutations.

Acknowledgements

This work was supported in part by the Coulter–Drexel Translational Research Partnership grant, the Nanotechnology Institute of Benjamin Franklin Partnership of Southeastern Pennsylvania, and the National Institute of Health Grants No. 1R41AI112224 and 1R41AI120445.

References

1 E. Crowley, F. Di Nicolantonio, F. Loupakis and A. Bardelli, *Nat. Rev. Clin. Oncol.*, 2013, **10**, 472–484.
2 E. G. Robertson and G. Baxter, *Clin. Radiol.*, 2011, **66**, 1007–1014.

3 R. H. Lipsky, C. M. Mazzanti, J. G. Rudolph, K. Xu, G. Vyas, D. Bozak, M. Q. Radel and D. Goldman, *Clin. Chem.*, 2001, **47**, 635–644.
4 F. Caruso, E. Rodda, D. N. Furlong, K. Niikura and Y. Okahata, *Anal. Chem.*, 1997, **69**, 2043–2049.
5 Y. H. Su, M. Wang, T. M. Block, O. Landt, I. Botezatu, O. Serdyuk, A. Lichtenstein, H. Melkonyan, L. D. Tomei and S. Umansky, *Ann. N. Y. Acad. Sci.*, 2004, **1022**, 81–89.
6 Y. H. Su, M. J. Wang, D. E. Brenner, A. Ng, H. Melkonyan, S. Umansky, S. Syngal and T. M. Block, *J. Mol. Diagn.*, 2004, **6**, 101–107.
7 S. R. Umansky and L. D. Tomei, *Expert Rev. Mol. Diagn.*, 2006, **6**, 153–163.
8 D. M. Hammond, A. Manetto, J. Gierlich, V. A. Azov, P. M. Gramlich, G. A. Burley, M. Maul and T. Carell, *Angew. Chem., Int. Ed.*, 2007, **46**, 4184–4187.
9 M. Passamano and M. Pighini, *Sens. Actuators, B*, 2006, **118**, 177–181.
10 K. Feng, J. Li, J. H. Jiang, G. L. Shen and R. Q. Yu, *Biosens. Bioelectron.*, 2007, **22**, 1651–1657.
11 R. Gasparac, B. J. Taft, M. A. Lapierre-Devlin, A. D. Lazareck, J. M. Xu and S. O. Kelley, *J. Am. Chem. Soc.*, 2004, **126**, 12270–12271.
12 S. J. Park, T. A. Taton and C. A. Mirkin, *Science*, 2002, **295**, 1503–1506.
13 L. He, M. D. Musick, S. R. Nicewarner, F. G. Salinas, S. J. Benkovic, M. J. Natan and C. D. Keating, *J. Am. Chem. Soc.*, 2000, **122**, 9071–9077.
14 X. Mao, L. Yang, X. L. Su and Y. Li, *Biosens. Bioelectron.*, 2006, **21**, 1178–1185.
15 L. K. Gifford, I. E. Sendroiu, R. M. Corn and A. Luptak, *J. Am. Chem. Soc.*, 2010, **132**, 9265–9267.
16 T. Yang, N. Zhou, Y. Zhang, W. Zhang, K. Jiao and G. Li, *Biosens. Bioelectron.*, 2009, **24**, 2165–2170.
17 G. Zheng, F. Patolsky, Y. Cui, W. U. Wang and C. M. Lieber, *Nat. Biotechnol.*, 2005, **23**, 1294–1301.
18 G. J. Zhang, Z. H. Luo, M. J. Huang, G. K. Tay and E. J. Lim, *Biosens. Bioelectron.*, 2010, **25**, 2447–2453.
19 A. Andreu, J. W. Merkert, L. A. Lecaros, B. L. Broglin, J. T. Brazell and M. El-Kouedi, *Sens. Actuators, B*, 2006, **114**, 1116–1120.
20 Z. Gao, A. Agarwal, A. D. Trigg, N. Singh, C. Fang, C. H. Tung, Y. Fan, K. D. Buddharaju and J. Kong, *Anal. Chem.*, 2007, **79**, 3291–3297.
21 J.-i. Hahm and C. M. Lieber, *Nano Lett.*, 2003, **4**, 51–54.
22 J. Wang, R. Polsky, A. Merkoci and K. L. Turner, *Langmuir*, 2003, **19**, 989–991.
23 H. Chang, Y. Yuan, N. Shi and Y. Guan, *Anal. Chem.*, 2007, **79**, 5111–5115.
24 M. Su, S. Li and V. P. Dravid, *Appl. Phys. Lett.*, 2003, **82**, 3562–3564.
25 K. Rijal and R. Mutharasan, *Anal. Chem.*, 2007, **79**, 7392–7400.
26 S. Zheng, J. H. Choi, S. M. Lee, K. S. Hwang, S. K. Kim and T. S. Kim, *Lab Chip*, 2011, **11**, 63–69.
27 J. Wang, A. N. Kawde and M. Musameh, *Analyst*, 2003, **128**, 912–916.
28 S. Husale, H. H. Persson and O. Sahin, *Nature*, 2009, **462**, 1075–1078.
29 T. Kurkina, A. Vlandas, A. Ahmad, K. Kern and K. Balasubramanian, *Angew. Chem., Int. Ed.*, 2011, **50**, 3710–3714.
30 C.-P. Chen, A. Ganguly, C.-Y. Lu, T.-Y. Chen, C.-C. Kuo, R.-S. Chen, W.-H. Tu, W. B. Fischer, K.-H. Chen and L.-C. Chen, *Anal. Chem.*, 2011, **83**, 1938–1943.
31 W. Gao, H. Dong, J. Lei, H. Ji and H. Ju, *Chem. Commun.*, 2011, **47**, 5220–5222.
32 L. Soleymani, Z. Fang, S. O. Kelley and E. H. Sargent, *Appl. Phys. Lett.*, 2009, **95**, 143701–143703.
33 O. A. Loaiza, S. Campuzano, M. Pedrero, M. I. Pividori, P. Garcia and J. M. Pingarron, *Anal. Chem.*, 2008, **80**, 8239–8245.
34 C. E. Kirimli, W. H. Shih and W. Y. Shih, *Analyst*, 2015, **140**, 1590–1598.
35 W. Y. Shih, H. Luo, H. Li, C. Martorano and W.-H. Shih, *Appl. Phys. Lett.*, 2006, **89**, 242913–242913.
36 W. Wu, C. E. Kirimli, W. H. Shih and W. Y. Shih, *Biosens. Bioelectron.*, 2013, **43**, 391–399.
37 C. E. Kirimli, W. H. Shih and W. Y. Shih, *Analyst*, 2014, **139**, 2754–2763.
38 Q. Zhu, W. Y. Shih and W. H. Shi, *Sens. Actuators, B*, 2009, **138**, 1–4.
39 Q. Zhu, W. Y. Shih and W.-H. Shih, *Appl. Phys. Lett.*, 2008, **92**, 183505.
40 W. Y. Shih, Q. Zhu and W. H. Shih, *J. Appl. Phys.*, 2008, 104.
41 Q. Zhu, W. H. Shih and W. Y. Shih, *Sens. Actuators, B*, 2013, **182**, 9.
42 W. Wu, W. Y. Shih and W. H. Shih, *J. Appl. Phys.*, 2013, 114.
43 V. Bazan, V. Agnese, S. Corsale, V. Calo, M. R. Valerio, M. A. Latteri, S. Vieni, N. Grassi, G. Cicero, G. Dardanoni, R. M. Tomasino, G. Colucci, N. Gebbia and A. Russo, *Ann. Oncol.*, 2005, **16**(Suppl 4), iv50–iv55.
44 S. Eser, A. Schnieke, G. Schneider and D. Saur, *Br. J. Cancer*, 2014, **111**, 817–822.
45 Y. Imamura, T. Morikawa, X. Liao, P. Lochhead, A. Kuchiba, M. Yamauchi, Z. R. Qian, R. Nishihara, J. A. Meyerhardt, K. M. Haigis, C. S. Fuchs and S. Ogino, *Clin. Cancer Res.*, 2012, **18**, 4753–4763.
46 S. A. Forbes, N. Bindal, S. Bamford, C. Cole, C. Y. Kok, D. Beare, M. Jia, R. Shepherd, K. Leung, A. Menzies, J. W. Teague, P. J. Campbell, M. R. Stratton and P. A. Futreal, *Nucleic Acids Res.*, 2011, **39**, D945–D950.
47 L. A. Ugozzoli, D. Latorra, R. Puckett, K. Arar and K. Hamby, *Anal. Biochem.*, 2004, **324**, 143–152.
48 L. S. Chou, C. Meadows, C. T. Wittwer and E. Lyon, *Bio-Techniques*, 2005, **39**, 644, 646, 648 passim.
49 M. P. Johnson, L. M. Haupt and L. R. Griffiths, *Nucleic Acids Res.*, 2004, **32**, e55.
50 E. Kierzek, A. Ciesielska, K. Pasternak, D. H. Mathews, D. H. Turner and R. Kierzek, *Nucleic Acids Res.*, 2005, **33**, 5082–5093.

51 A. A. Koshkin, S. K. Singh, P. Nielsen, V. K. Rajwanshi, R. Kumar, M. Meldgaard, C. E. Olsen and J. Wengel, *Tetrahedron*, 1998, **54**, 3607–3630.
52 H. Orum, M. H. Jakobsen, T. Koch, J. Vuust and M. B. Borre, *Clin. Chem.*, 1999, **45**, 1898–1905.
53 A. Simeonov and T. T. Nikiforov, *Nucleic Acids Res.*, 2002, **30**, e91.
54 N. Tolstrup, P. S. Nielsen, J. G. Kolberg, A. M. Frankel, H. Vissing and S. Kauppinen, *Nucleic Acids Res.*, 2003, **31**, 3758–3762.
55 Y. You, B. G. Moreira, M. A. Behlke and R. Owczarzy, *Nucleic Acids Res.*, 2006, **34**, e60.
56 M. A. Land, J. Webster, A. Christoforou, D. Praveen, P. Jeffery, J. Chalmers, W. Smith, M. Woodward, F. Barzi, C. Nowson, V. Flood and B. Neal, *BMJ Open*, 2014, **4**, e003720.
57 MD-Health. http://www.md-health.com/Normal-Urine-Output.html, David C. Dugdale, III, MD, Professor of Medicine, Division of General Medicine, Department of Medicine, University of Washington School of Medicine. Also reviewed by David Zieve, MD, MHA, Bethanne Black, and the A.D.A.M. Editorial team.
58 C. E. Kirimli, W. H. Shih and W. Y. Shih, *Analyst*, 2013, **138**, 6117–6126.
59 M. C. Soylu, W.-H. Shih and W. Y. Shih, *Ind. Eng. Chem. Res.*, 2013, **52**, 2590–2597.
60 M. Ç. Soylu, *Piezoelectric Plate Sensor for in situ Genetic Detection of Hepatitis B Virus in Serum without DNA Isolation and Amplification*, Drexel University, 2013.